Available online at www.sciencedirect.com
ScienceDirect
Trans. Nonferrous Met. Soc. China 35(2025) 2320−2331
Transactions of Nonferrous Metals Society of China
www.tnmsc.cn

Influence of ordering behaviors on thermodynamic and mechanical properties of FCC_CoNiV multi-principal element alloys

Chu-bo ZHANG[1], Cheng QIAN[2], Zi-an YE[2], Pan-hong ZHAO[1], Rong CHEN[2], Bo WU[1,2], Yang QIAO[1], Liang-ji WENG[1], Long-ju SU[2], Tian-liang XIE[2], Bai-sheng SA[2], Yu LIU[3], Chun-xu WANG[3]

1. Materials Design and Manufacture Simulation Facility, School of Advance Manufacturing, Fuzhou University, Jinjiang 362200, China;
2. Multiscale Computational Materials Facility & Materials Genome Institute, School of Materials Science and Engineering, Fuzhou University, Fuzhou 350100, China;
3. Institute of High Temperature Alloy, Central Iron & Steel Research Institute Group, Beijing 100081, China

Received 1 November 2023; accepted 26 June 2024

Abstract: In order to understand the influence of ordering behaviors on the thermodynamic and mechanical properties of multi-principal element alloys (MPEAs), the temperature-dependent thermodynamic properties and mechanical properties of FCC_CoNiV MPEAs were comparatively predicted, where the alloys were modeled as the ordered configurations based on our previously predicted site occupying fractions (SOFs), as well as disordered configuration based on traditional special quasi-random structure (SQS). The ordering behavior not only improves the thermodynamic stability of the structure, but also increases the elastic properties and Vickers hardness. For example, at 973 K, the predicted bulk modulus (B), shear modulus (G), Young's modulus (E), and Vickers hardness (H_V) of FCC_CoNiV MPEA based on SOFs configuration are 187.82, 79.03, 207.93, and 7.58 GPa, respectively, while the corresponded data are 172.58, 57.45, 155.14, and 4.64 GPa for the SQS configuration, respectively. The Vickers hardness predicted based on SOFs agrees considerably well with the available experimental data, while it is underestimated obviously based on SQS.

Key words: FCC_CoNiV; multi-principal element alloys (MPEAs); ordering behavior; temperature-dependent properties; computational materials science

1 Introduction

Multi-principal element alloys (MPEAs) are also named composition complex alloys (CCAs), high entropy alloys (HEAs), or medium entropy alloys (MEAs), depending on the number of multi-principal components, which consist of various elements in equal or approximately equal proportions [1−3]. It is believed that some of the MPEAs may hold one or more outstanding properties at low or even high temperatures. These properties include high yield strength, elastic modulus and hardness, good fracture toughness, good resistance to oxidation, corrosion, and even radiation damage, and soft magnetic properties [4−6]. For example, FCC_CoCrFeMnNi MPEA exhibits exceptional damage tolerance, with tensile strength exceeding 1 GPa and fracture toughness exceeding 200 MPa·m$^{1/2}$ [7]. AlCoCrFeNi exhibits exceptional wear resistance compared to CoCrFeMnNi at 300, 600, and 900 °C, which also has a superior microhardness of HV 630 at room temperature [8]. What's more, $Al_xCr_yMo_zNbTiZr$

Corresponding author: Bo WU, Tel: +86-13023819517, E-mail: wubo@fzu.edu.cn, ORCID: 0000-0002-7676-2736;
Bai-sheng SA, E-mail: bssa@fzu.edu.cn
https://doi.org/10.1016/S1003-6326(25)66817-8

MPEAs contain the potential of high temperature oxidation behavior for its protective oxide layer [9]. Especially, the FCC_CoNiV MPEA has received intensive investigations recently since SOHN et al [10] reported a trade-off of the yield strength and ductility due to the severe lattice distortion, while the strength was affected considerably by the grain size [11]. NUTOR et al [12] found that CoNiV may have high strength and ductility even at liquid helium temperature (4.2 K). Thus, FCC_CoNiV MPEA shows potential application prospects [10−12]. However, the systematical thermodynamic and mechanical properties at definite temperatures are still rare. It is urgent to obtain sufficient fundamental data for engineering applications.

In the past decade, computational materials science played ever-increasing role in exploration of the advanced materials [13−15]. The elastic properties, which refer to a material's ability to return to its original shape after being stressed, are crucial indicators of mechanical performance in materials [16]. Considering the application circumstance, the temperature-dependent elastic properties are crucial for material design [17−19].

MPEAs were previously believed as a kind of random solid solution, however, due to the existence of the difference among different types of the multi-principal constituent alloying elements, as well as among different types of the constituent sublattices of the crystal lattice structure of the alloy phase. The site preferences of the atoms occupying the sublattice are inevitably at definite temperatures, which are also known as the ordering behavior. In this work, we focused on the effect of the site preference behaviors on the thermodynamic and mechanical properties at definite temperatures.

The predominant influence on the temperature-dependent elastic properties is the change in the volume of the unit cell. Here, we employed quasi-harmonic approximation (QHA) method [20,21] to study the thermodynamics and elastic properties at definite temperatures. We consider only lattice thermal expansion due to constraints on available computing resources, without further exploring lattice vibration behaviors using AIMD simulation [22,23]. According to a previously published work within our group on the temperature-dependent thermodynamics and elastic properties of FCC_CoCrFeNi MPEA [24], it was found that the related data may vary by 1%−10% depending on the different properties and specific temperatures. Additionally, the ordered structure shows better stability in thermodynamics and larger elastic properties. Since we aim to address the significant influence of ordering behaviors on the thermodynamic and mechanical properties of multi-principal element alloys, we rationally omitted the AIMD part in the case of computing resource limitation. However, it is necessary to consider the lattice vibration behaviors precisely by employing the AIMD approach in our further work based on site preference.

The site preferences have been quantitatively described using the site occupying fractions (SOFs) in the sublattice model following the crystallographic information strictly. Till now, the temperature- and composition-dependent SOFs of some typical intermetallic compounds with two sublattice model for $L1_2$ [25−27] and C15 [28,29] phases, three sublattice model [30−32] or four sublattice model [33], and the general characterization approaches [34,35], as well as some typical systems of HEAs/MPEAs [36−38] have been reported. Recently, the experimental evidence stimulated the hot topics so-called chemical short-range order (CSRO) or local chemical order (LCO), with heated arguments [39−42]. In fact, the CSRO or LCO behaviors are affected by many factors, such as inhomogeneous fabrication under insufficient smelting temperature or heat treatment time, site preference, and even the precipitating second phase at the phase equilibrium state. DING et al [39] proved that CSRO is thermodynamically favored in high-entropy alloys (HEAs) which can be adjusted and thus affect the mechanical behavior of these alloys. Unraveling the internal ordering behavior in MPEAs has become an interesting and fundamental issue among researchers [43−45]. CHEN et al [41,42] observed CSRO directly in FCC_CoNiV MPEA, and it is shown that the CSRO behavior is caused by the V—Co bond and V—Ni bond preference and V—V bond avoidance, which agrees well with the results of our previous theoretical work of FCC_CoNiV MPEA with $(V_{1.000})_{1a}(Co_{0.444}Ni_{0.444}V_{0.112})_{3c}$ configuration, where all the 1a sublattice sites (angular position of the FCC unit cell) are occupied by V atoms, and the rest V atoms (a quarter of all the V atoms) occupy the 3c sublattice (face center position) [37]. Thus, the common modeling

methods for MPEAs, such as special quasi-random structure (SQS) [46], are not the reasonable models to accurately reflect the distribution of atoms in the crystal lattice structure.

In this work, we carried out a comparative study of the temperature-dependent thermodynamic properties and elastic properties of FCC_CoNiV MPEA with the ordered configurations $(V_{1.0000})_{1a}$-$(Co_{0.4445}Ni_{0.4444}V_{0.1111})_{3c}$ (representing a considerably ordered FCC structure) based on our previously rationally predicted site occupying fractions (SOFs) previously [37], as well as the disordered configuration $(Co_{0.3333}Ni_{0.3333}V_{0.3334})_{1a}(Co_{0.3333}$-$Ni_{0.3333}V_{0.3334})_{3c}$ (representing a disordered FCC structure) based on the traditional SQS, which hypothesized the alloy holding a perfectly random structure. Based on the first-principles calculations at the ground state and at definite temperatures, the total energy, temperature-dependent lattice parameters, thermodynamic properties, and mechanical properties of the ordered and disordered FCC_CoNiV MPEAs were predicted and discussed.

2 Structural model and computing method

2.1 Structural model of ordered and disordered structure of FCC_CoNiV MPEA

Our previous study of the site preference of FCC_CoNiV MPEA shows that there is a significant ordered behavior with $(V_{1.000})_{1a}$-$(Co_{0.444}Ni_{0.444}V_{0.112})_{3c}$ at all considered heat treatment temperature ranges [37], which deviates obviously from the random mixing structure, that is, V atoms occupy all the 1a sublattices (angular position of FCC) exclusively, and rest of V atoms and all the Co and Ni atoms randomly occupy 3c sublattices (face-centered position of FCC). In the following model, considering the available computing power to calculate the temperature-dependent thermodynamics and elastic properties, as well as modelling the ternary equimolar composition, we constructed 2×2×3 supercells based on the $L1_2$_$AuCu_3$ prototype structure, which corresponds to the ordered FCC structure, and totally there are 48 atoms in the supercell. It is worth noting that for FCC_CoNiV MPEAs, the previously predicted temperature-independent site occupancy behavior brings us convenience. We only need to establish one type of atomic distribution configuration for the ordered structure at all relevant heat treatment temperatures. Alternatively, various site occupancy configurations should be established according to the varying site occupancy behaviors at different heat treatment temperatures, based on the defined temperature-dependent SOFs for the studied MPEAs. For comparison, we constructed a disordered 2×2×3 supercells of FCC_CoNiV MPEA based on SQS [46] using the ATAT software package [47].

To represent the disordered structure, we need also to establish only one kind of atom distributing configuration for the disordered structure used at all concerned heat treatment temperature because it is assumed as a perfect random structure at all concerned heat treatment temperatures. It is evident that the only distinction between the SOFs model and the SQS model lies in the distribution of atoms on the atom positions of the supercell of $L1_2$ structure. When fulfilling the crystal lattice relaxing calculation to characterize the lattice distortion, we adopted the selective dynamics approach, where we fixed one of the atoms as the original point to avoid the swift of the full lattice, and guided three selective atoms sliding along the direction of *X*, *Y*, and *Z* axis, respectively, to avoid the rotation of the full crystal lattice structure which may complex the characterization of lattice distortion, while the rest 44 atoms were allowed to relax freely. The ordered and disordered supercell models are shown in Fig. 1, and the formatted crystal lattice structure file (POSCAR) called in current calculations is provided in Part I of Supplementary Materials (ESM).

2.2 First-principles and phonon calculations

All the first-principles calculations at the ground state were fulfilled using the Vienna Ab initio Simulation Package (VASP) based on the density functional theory (DFT) [48−50]. The ion−electron interaction was described by the generalized gradient approximation (GGA) and the projection augmented wave (PAW) method [49]. The GGA of the Perdew-Burk-Ernzerhof (PBE) was used to describe the exchange−correlation function [50,51]. The energy convergences of the optimization calculation at the ground and the phonon calculation were both set to be 1×10^{-5} eV, and the cut-off energy setting was set to be 450 eV.

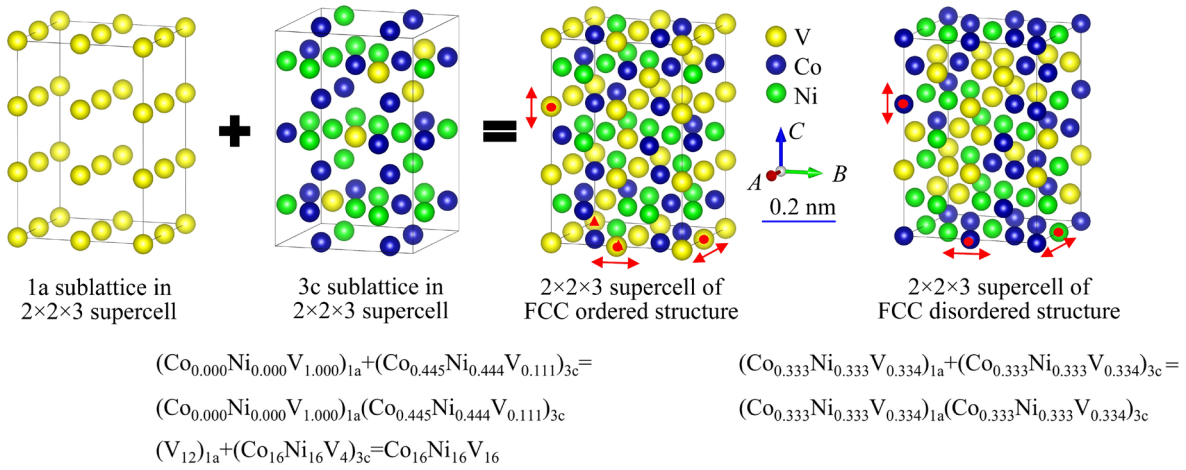

Fig. 1 Ordered model based on SOFs and disordered model based on SQS of FCC_CoNiV MPEA established using 2×2×3 supercell of $L1_2$ structure (The red triangle mark represents the fixed origin, the red dot represents the manual-guiding sliding atom, and the red double-headed arrow represents the slip directions allowed): (a) Ordered FCC_CoNiV MPEA based on SOFs; (b) Disordered FCC_CoNiV MPEA based on SQS

The ordered and disordered configurations only consider the ferromagnetic state in all calculations, achieved by setting ISPIN=2 in the INCAR file prepared for VASP, and all calculation settings ensure that the convergence threshold of the total energy at the ground state is set to be less than 1 meV/atom.

Strictly speaking, the FCC_CoNiV was now modeled as tetragonal structure rather than an FCC structure, which led to an increased number of isolating elastic constants from three to six. Based on the relationship between strain energy and strain, the elastic properties of the ordered and disordered FCC_CoNiV MPEAs at the ground state were predicted and compared with the available experimental literature.

Due to the limitation of the available computing power at the moment, the temperature-dependent thermodynamic properties and mechanical properties of the ordered and disordered FCC_CoNiV MPEAs were predicted based on the quasi-harmonic approximation (QHA), where the properties were mainly determined by volume changes caused by thermal expansion although the thermal-electron contribution and lattice vibration should also be considered further to obtain more accurate predicted results for the temperature-dependent elastic properties [19]. Therefore, prediction of temperature-dependent equilibrium volume is essential to predict the temperature-dependent mechanical properties. The temperature-dependent thermodynamic properties and equilibrium volume of the ordered and disordered FCC_CoNiV MPEAs were obtained using density functional perturbation theory (DFPT) based on QHA. The Brillouin region sampling (KPOINTS) was set to be a 3×3×2 Monkhorst- Pack grid [52]. The temperature-dependent thermo- dynamic and thermophysical properties at definite temperatures were calculated by combining VASP with PHONOPY software package.

3 Results and discussion

3.1 Crystal lattice parameters, and elastic constants of FCC_CoNiV MPEAs at ground state

The calculated crystal lattice parameters and total energies of FCC_CoNiV MPEA are presented in Table 1. The results show that the total energy of the ordered structure is smaller than that of the disordered structure, indicating that the ordered structure based on SOFs is more stable thermodynamically than the disordered structure based on SQS. Meanwhile, the volume of the ordered structure based on SOFs is smaller than that of the disordered structure based on SQS. Due to the lattice distortion, the crystal lattice structure tends to deform slightly to a triclinic structure, with the angles deviating from 90° by less than 0.25°, which can be omitted.

The elastic properties of the ordered and

disordered FCC_CoNiV MPEAs at the ground state are predicted and compared with the available experimental literature, seen in Table 2.

From Table 2, it is seen that the calculated elastic constants of the FCC_CoNiV MPEAs at the ground state based on SOFs using a 2×2×3 supercell agree well with our previous results using a 3×3×3 supercell [37]. Of these, C_{44} has the largest deviation of 6.56%, and for C_{11} and C_{12}, the deviation is less than 2%. The elastic constants of the FCC_CoNiV MPEAs at the ground state calculated based on the 2×2×3 disordered supercell are in good agreement with those by ZHOU et al [53], with a maximum deviation in C_{44} of only 2.60%. The calculated elastic constants (C_{11}, C_{12}, and C_{44}) of the tetragonal FCC_CoNiV MPEAs are also applicable to FCC_CoNiV MPEAs. It is found that except the elastic constant of C_{13}, the rest of elastic constants of the FCC_CoNiV MPEA based on SOFs configuration are larger than those based on SQS configurations at the ground state. Among them, the elastic constant of C_{11} represents the linear compression along the X-axis, and the larger the value, the greater the stiffness. The elastic constant of C_{44} is the indentation hardness of the solid, and the larger the value, the stronger the ability of a material to resist shear deformation of the (100) crystal plane is. Therefore, combined with the predicted elastic constants of C_{11} and C_{44}, it is found that the ordered configuration has greater stiffness and stronger resistance to (100) crystal plane shear deformation. For the tetragonal crystal lattice structure, its stability criterion is different from that of face-centered cubic or body-centered cubic structure, and the Born elastic stability criteria are shown in Eqs. (1)−(3) [54−57]:

$$C_{11}>0,\ C_{33}>0,\ C_{44}>0,\ C_{66}>0 \tag{1}$$

$$(C_{11}-C_{12})>0,\ (C_{11}+C_{33}-2C_{13})>0 \tag{2}$$

$$2(C_{11}+C_{12})+C_{33}+4C_{33}>0 \tag{3}$$

By examining the corresponding data, it is concluded that both the ordered and disordered FCC_CoNiV MPEAs satisfy the Born elastic stability criteria at the ground state, indicating that both the ordered and disordered FCC_CoNiV multi-principal element alloys are mechanically stable at the ground state.

3.2 Temperature-dependent thermodynamic properties of FCC_CoNiV MPEAs

The temperature-dependent thermodynamic properties and equilibrium volume of the ordered and disordered FCC_CoNiV MPEAs are obtained using density functional perturbation theory (DFPT) based on QHA, which are shown in Fig. 2 and Part II of Supplementary Materials, respectively. These predicted thermodynamic properties include the temperature-dependent Gibbs free energy, entropy, heat capacity, and thermal expansion coefficient.

Figure 2(a) shows the temperature-dependent Gibbs free energy of the ordered and disordered FCC_CoNiV MPEAs. The Gibbs free energy of the ordered and disordered FCC_CoNiV MPEAs decreases with increasing temperature, and the temperature-dependent Gibbs free energy of the

Table 1 Crystal lattice parameters and total energies of ordered structure of FCC_CoNiV MPEAs based on SOFs and disordered structure based on SQS at ground state using 2×2×3 supercells based on $L1_2$ unit cell

Configuration	a/Å	b/Å	c/Å	α/(°)	β/(°)	γ/(°)	V/Å^3	E_{tot}/eV
SOFs	7.075	7.071	10.772	90.110	89.951	90.204	538.914	−350.353
SQS	7.214	7.107	10.661	90.008	90.103	89.900	546.584	−346.528

Table 2 Elastic constants of FCC_CoNiV MPEAs at ground state for ordered states based on SOFs and disordered states based on SQS at ground state

Configuration (Number of atoms involved)	C_{11}/GPa	C_{12}/GPa	C_{13}/GPa	C_{33}/GPa	C_{44}/GPa	C_{66}/GPa	Supercell size	Source
SOFs (48)	295.59	188.75	182.81	296.20	130.10	140.35	2×2×3	This work
SOFs (108)	300.11	185.19	−	−	138.64	−	3×3×3	[37]
SQS (48)	254.29	175.59	184.32	256.93	106.24	109.96	2×2×3	This work
SQS	251.00	173.00	−	−	109.00	−		[53]

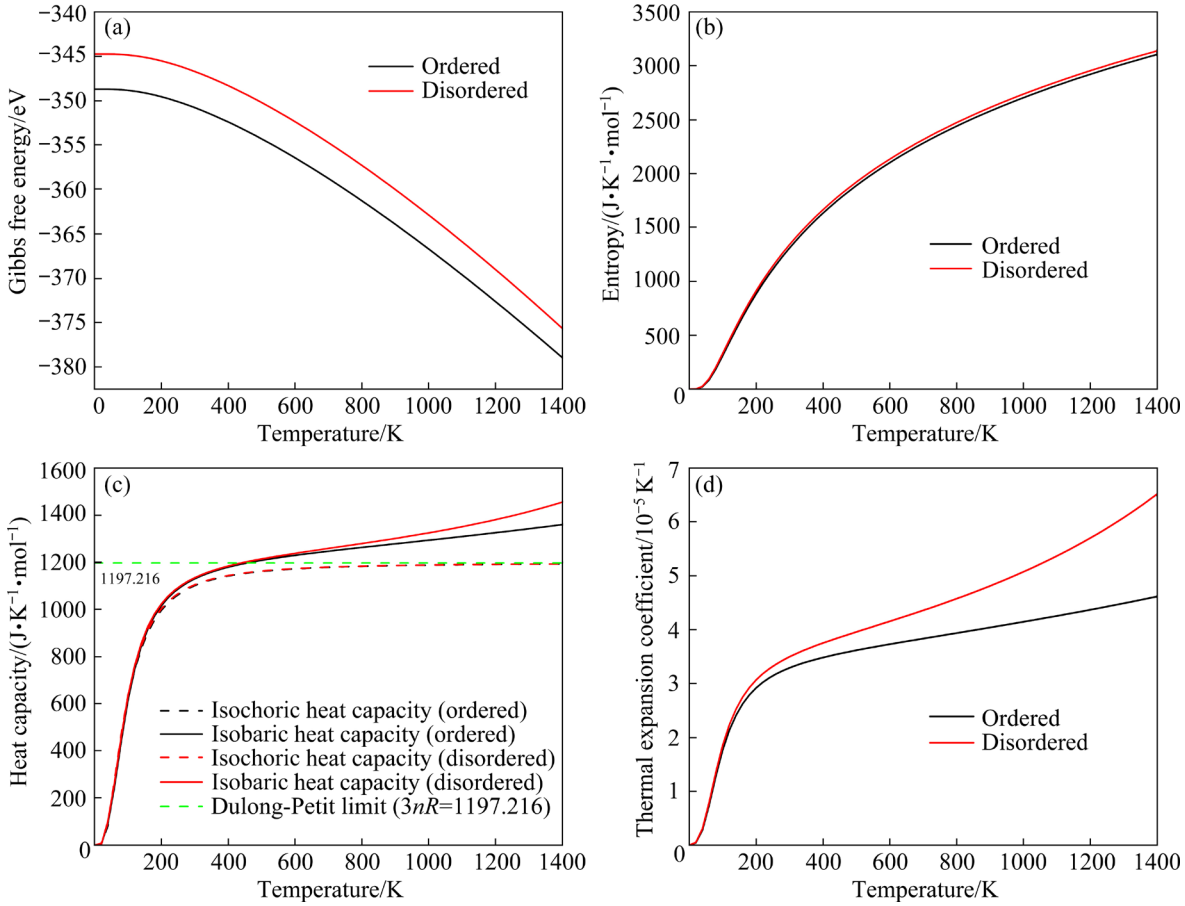

Fig. 2 Temperature-dependent thermodynamic properties of ordered and disordered FCC_CoNiV MPEAs: (a) Gibbs free energy; (b) Entropy; (c) Isobaric capacity and isochoric heat capacity; (d) Thermal expansion coefficient

ordered configuration is lower than that of the disordered configuration, indicating that the ordered FCC_CoNiV multi-principal element alloy is more stable than the disordered state thermodynamically. Figure 2(b) displays the related temperature-dependent entropy, which increases for both the ordered and disordered configurations as the temperature rises. The entropy of the ordered configuration is slightly smaller than that of the disordered configuration. Figure 2(c) shows the temperature-dependent isochoric heat capacity (C_θ) and isobaric heat capacity (C_p) of the related configurations, respectively. It is seen that as the temperature increases, all the heat capabilities increase rapidly when the temperature is below 200 K. Both the ordered and disordered FCC_CoNiV MPEAs exhibit almost the similar heat capacities. However, as the temperature further increases, the isochoric heat capacities of both the ordered and disordered configurations reach a constant value of 1197.216 J/(K·mol) at high temperatures, satisfying the Dulong-Petit Limit: C_θ=3nR, where n is the total number of atoms in the system, and R is the molar gas constant. However, the isobaric heat capacity of the disordered configuration and the ordered configuration are similar when the temperature is below 600 K, and beyond 600 K, the isobaric heat capacity of the disordered configuration gradually exceeds that of the ordered configuration. Figure 2(d) shows the related temperature-dependent thermal expansion coefficients, where the change trends are similar to those of the isobaric heat capacities. The thermal expansion coefficients of both the ordered and disordered configurations increase rapidly with temperatures below 200 K, and beyond 200 K, the thermal expansion coefficients of the disordered configuration are larger those of the ordered configuration.

There are some inherent relationships between the temperature-dependent volume and the temperature-dependent thermal expansion

coefficient, and some complex transformations are involved when performing the calculations. Thus, the temperature-dependent volume and temperature-dependent thermal expansion coefficient reflect each other. Since the data are indispensable for further calculations at definite temperatures, to read the data easily, the directly calculated results of the temperature-dependent equilibrium volumes of the ordered and disordered FCC_CoNiV MPEAs are shown in Fig. S1 in Supplementary Materials. The equilibrium volume of ordered configuration is smaller than that of the disordered configuration across all temperature ranges. Below 800 K, the temperature−volume curves of the ordered and disordered configurations are almost parallel, indicating similar growth rates. However, above 800 K, the volume growth rate of the disordered configuration increases gradually.

3.3 Temperature-dependent mechanical properties of FCC_CoNiV MPEAs

Based on the predicted temperature-dependent equilibrium volume, the predicted temperature-dependent elastic constants of the ordered and disordered FCC_CoNiV MPEAs based on QHA are shown in Figs. 3(a) and (b) respectively. It is seen that the polycrystalline elastic constants of both the ordered and disordered FCC_CoNiV MPEAs show a nearly linear decreasing trend with increasing temperature, which may be attributed to the thermal expansion effect at high temperature that weakens the covalent bonds between atoms. Except for the elastic constant of C_{13}, the remaining temperature-dependent elastic constants of the ordered FCC_CoNiV MPEAs surpass those of the disordered configuration at all temperatures. The temperature-dependent elastic constants of both configurations satisfy the Born elastic stability criteria, which means they are mechanically stable at definite temperatures.

The elastic modulus of the material can be further deduced from the elastic constant. The relationship between the polycrystalline elastic moduli and elastic constants of the tetragonal structure are different from that of the face-centered cubic (FCC) and body-centered cubic (BCC) structures. Through Voigt-Reuss-Hill approximation, the bulk modulus (B), shear modulus (G), and Young's modulus (E) of the tetragonal structure can be obtained through the elastic constants based on

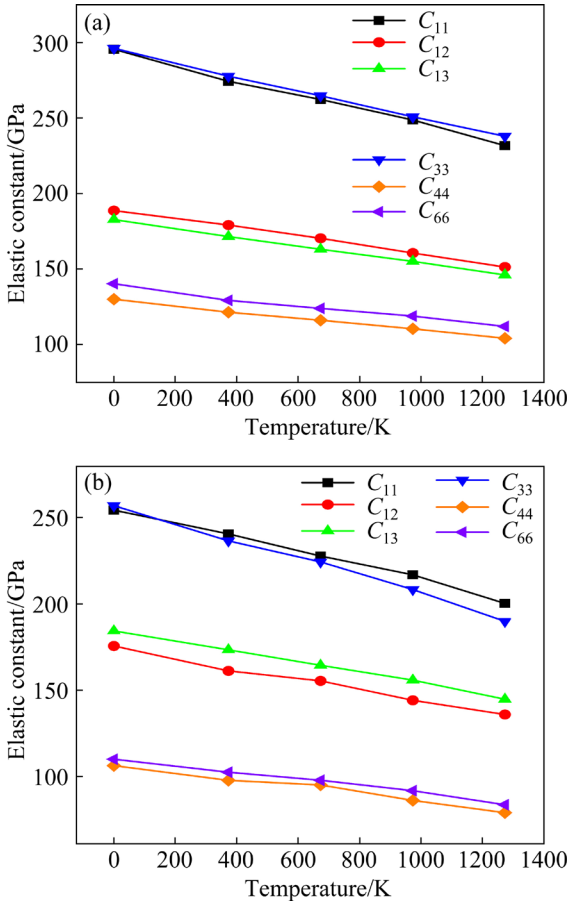

Fig. 3 Temperature-dependent elastic constants of ordered (a) and disordered (b) FCC_CoNiV MPEAs

Eqs. (4)−(9) [57−59]:

$$M=C_{11}+C_{12}+2C_{33}-4C_{13} \tag{4}$$

$$C^2=(C_{11}+C_{12})C_{33}-2C_{13}^2 \tag{5}$$

$$B_V=[2(C_{11}+C_{12})+C_{33}+4C_{13}]/9 \tag{6}$$

$$G_V=[M+3C_{11}-3C_{12}+12C_{44}+6C_{66}]/30 \tag{7}$$

$$B_R=C^2/M \tag{8}$$

$$G_R=15\left(\frac{18B_V}{C^2}+\frac{6}{C_{11}-C_{12}}+\frac{6}{C_{44}}+\frac{3}{C_{66}}\right)^{-1} \tag{9}$$

where B_V is the Voigt approximation value of bulk modulus, G_V is the Voigt approximation value of shear modulus, B_R is the Reuss approximation value of bulk modulus, and G_R is the Reuss approximation value of shear modulus, respectively.

$$B=0.5(B_V+B_R) \tag{10}$$

$$G=0.5(G_V+G_R) \tag{11}$$

where Eqs. (10) and (11) are based on Hill average.

$$E=\frac{9BG}{3B+G} \tag{12}$$

Table 3 Temperature-dependent mechanical properties of ordered and disordered FCC_CoNiV MPEAs

Structure model	Temperature/K	Pugh's ratio, k	Bulk modulus, B/GPa	Poisson's ratio, v	Young's modulus, E/GPa	Shear modulus, G/GPa	Source
SOFs	0	0.42	221.79	0.31	246.70	93.83	This work
SOFs	0	0.43	223.28	0.31	255.09	97.12	Ref. [37]
SQS	0	0.34	205.92	0.35	188.52	69.95	This work
SOFs	373	0.42	207.89	0.32	227.99	86.54	This work
SQS	373	0.30	192.55	0.36	175.34	65.03	This work
SOFs	673	0.42	198.11	0.32	218.55	83.03	This work
SQS	673	0.34	183.11	0.35	167.26	62.05	This work
SOFs	973	0.42	178.82	0.32	207.93	79.03	This work
SQS	973	0.33	172.58	0.37	155.14	57.45	This work
SOFs	1273	0.42	176.55	0.32	194.92	74.06	This work
SQS	1273	0.32	160.11	0.37	140.61	51.94	This work

In addition to the equations mentioned above (Eqs. (6) and (7)), Pugh's ratio (k) and Poisson's ratio (v) are calculated by these equations [57−59]:

$$k=G/B \quad (13)$$

$$v=(3-2k)/[2(3+k)] \quad (14)$$

The Vickers hardness (H_V) of ordered and disordered FCC_CoNiV MPEAs are calculated with TIAN's model [56]:

$$H_V=0.92k^{1.137}G^{0.708} \quad (15)$$

Based on the above empirical equations (4)−(15), all the bulk modulus (B), shear modulus (G), and Young's modulus (E) of ordered and disordered tetragonal MPEA CoNiV at the ground state and finite temperature are given in Table 3. The temperature-dependent Vickers hardness of FCC_CoNiV MPEA with ordered or disordered configuration is shown in Fig. 4.

It is seen that the predicted temperature-dependent bulk modulus, shear modulus, and Young's modulus of the FCC_CoNiV MPEA at all temperatures are larger than those of disordered configuration. This indicates that the ordered configuration exhibits good resistance to the compression deformation, shear deformation, and volume change. Therefore, the ordered FCC_CoNiV MPEA has better temperature-dependent mechanical properties than its disordered configuration. As a result, the site preference behaviors of atoms on the sublattices stabilize not only the crystal lattice structure from the viewpoint of thermodynamics but also enhance the elastic properties compared to the corresponding hypothesized perfectly random structure. The limited experimental result concerns the Vickers hardness [59], which is used to verify the validity of the ordered and disordered structure models. It is evident that the Vickers hardness of the ordered configuration based on SOFs agrees considerably with the available experimental data [59], while it is underestimated obviously when using disordered configuration. The Vickers hardness decreases significantly with the increase in temperature for both the ordered and disordered structure models.

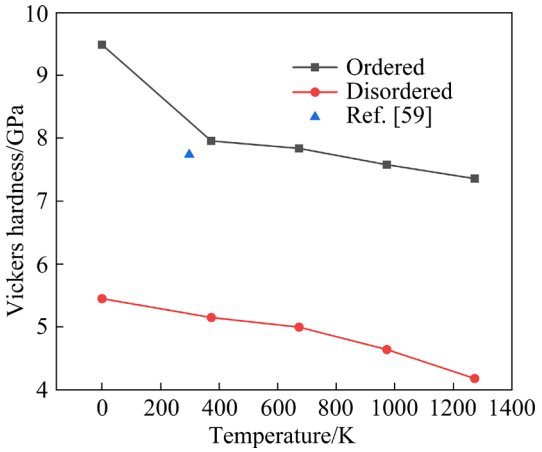

Fig. 4 Temperature-dependent Vickers hardness of ordered and disordered FCC_CoNiV MPEAs

4 Conclusions

(1) The ordered configuration based on SOFs model is $(V_{1.0000})_{1a}(Co_{0.4445}Ni_{0.4444}V_{0.1111})_{3c}$, while the

disordered configuration based on SQS model is $(Co_{0.3333}Ni_{0.3333}V_{0.3334})_{1a}(Co_{0.3333}Ni_{0.3333}V_{0.3334})_{3c}$.

(2) The total energy at the ground state and Gibbs free energies at all specified temperatures are lower for the ordered configuration compared to the disordered configuration, indicating better thermodynamic stability of ordered configuration.

(3) The predicted elastic properties and hardness decrease with increasing temperature for both the ordered and disordered structures. Except for the elastic constant of C_{13}, the ordered structure shows considerably greater mechanical properties (elastic constants, bulk modulus, shear modulus, Young's modulus, and Vickers hardness) compared to those of the disordered configurations.

(4) At 973 K, the predicted bulk modulus (B), shear modulus (G), Young's modulus (E), and Vickers hardness (H_V) of FCC_CoNiV MPEA based on SOFs configuration are 187.82, 79.03, 207.93, and 7.58 GPa, respectively, while the corresponding data are 172.58, 57.45, 155.14, and 4.64 GPa for the SQS configuration, respectively. The predicted Vickers hardness of the ordered structure agrees well with the experimental data, while it is noticeably underestimated based on the disordered structure.

CRediT authorship contribution statement

Chu-bo ZHANG: Formal analysis, Writing − Original draft; **Cheng QIAN:** Writing − Review & editing; **Zi-an YE:** Investigation; **Pan-hong ZHAO:** Data processing; **Rong CHEN:** Methodology; **Bo WU:** Funding acquisition, Conceptualization, Validation, Supervision, Project administration; **Yang QIAO:** Data curation, Software; **Liang-ji WENG:** Investigation; **Long-ju SU:** Investigation; **Tian-liang XIE:** Investigation; **Bai-sheng SA:** Writing − Review & editing; **Yu LIU:** Funding acquisition; **Chun-xu WANG:** Investigation, Funding acquisition, Supervision.

Declaration of competing interest

The authors declare that they have no known competing financial interests or personal relationships that could have appeared to influence the work reported in this paper.

Acknowledgments

This work was financially supported by the State Administration for Market Regulation, China (No. 2021MK050), the National Natural Science Foundation of China (Nos. 50971043, 51171046, 21973012), the Key Research and Development Program of China (Nos. 2022YFB3807200, CISRI-21T62450ZD), the Natural Science Foundation of Fujian Province, China (Nos. 2021J01590, 2020J01351, 2018J01754, 2020J01474), the Student Research and Training Program (SRTP) of Fuzhou University, China (No. 29320), and Fujian Provincial Department of Science & Technology, China (No. 2021H6011).

Supplementary Materials

The Supplementary Materials in this paper can be found at: http://tnmsc.csu.edu.cn/download/14-p2320-2023-1250-Supplementary-Materials.pdf.

References

[1] CANTOR B, CHANG I T H, KNIGHT P, VINCENT A J B. Microstructural development in equiatomic multicomponent alloys [J]. Materials Science and Engineering A, 2004, 375/376/377: 213−218.

[2] YEH J W, CHEN S K, LIN S J, GAN J Y, CHIN T S, SHUN T T, TSAU C H, CHANG S Y. Nanostructured high-entropy alloys with multiple principal elements: Novel alloy design concepts and outcomes [J]. Advanced Engineering Materials, 2004, 6: 299−303.

[3] OTTO F, YANG Y, BEI H, GEORGE E P. Relative effects of enthalpy and entropy on the phase stability of equiatomic high-entropy alloys [J]. Acta Materialia, 2013, 61: 2628−2638.

[4] CHEN Ping-hu, LI Bai-chun, LIU Zhen, ZHOU Ying-hao, LI Rui-qing, ZHANG Yun. High-temperature oxidation behaviors and mechanical properties of TiAlCrMn HEAs during heat treatment [J]. Transactions of Nonferrous Metals Society of China, 2024, 34: 203−218.

[5] WANG Hao, CHEN Wei-ping. Mechanical and corrosion properties of lightweight $(Ti_{60}Cr_{30}Nb_{10})_{100-x}Al_x$ medium-entropy alloys [J]. Transactions of Nonferrous Metals Society of China, 2024, 34: 219−235.

[6] EL A O, VO H T, TUNES M A, LEE C, ALVARADO A, KRIENKE N, POPLAWSKY J D, KOHNERT A A, GIGAX J, CHEN W Y, LI M, WANG Y Q, WRÓBEL J S, NGUYEN-MANH D, BALDWIN J K S, TUKAC O U, AYDOGAN E, FENSIN S, MARTINEZ E. A quinary WTaCrVHf nanocrystalline refractory high-entropy alloy withholding extreme irradiation environments [J]. Nature Communications, 2023, 14: 2516.

[7] GLUDOVATZ B, HOHENWARTER A, CATOOR D, CHANG E H, GEORGE E P, RITCHIE R O. A fracture-resistant high-entropy alloy for cryogenic applications [J]. Science, 2014, 345: 1153−1158.

[8] JOSEPH J, HAGHDADI N, SHAMLAYE K, HODGSON P, BARNETT M, FABIJANIC D. The sliding wear behaviour of CoCrFeMnNi and Al_xCoCrFeNi high entropy alloys at elevated temperatures [J]. Wear, 2019, 428: 32−44.

[9] WASEEM O A, AUYESKHAN U, LEE H M, RYU H J. A

combinatorial approach for the synthesis and analysis of $Al_xCr_yMo_zNbTiZr$ high-entropy alloys: Oxidation behavior [J]. Journal of Materials Research, 2018, 33: 3226−3234.

[10] SOHN S S, KWIATKOWSKI D S A, IKEDA Y, KÖRMANN F, LU Wen-jun, CHOI W S, GAULT B, PONGE D, NEUGEBAUER J, RAABE D. Ultrastrong medium-entropy single-phase alloys designed via severe lattice distortion [J]. Advanced Materials, 2019, 31: 1807142.

[11] SOHN S S, KIM D G, JO Y H, DA SILVA A K, LU Wen-jun, BREEN A J, GAULT B, PONGE D. High-rate superplasticity in an equiatomic medium-entropy VCoNi alloy enabled through dynamic recrystallization of a duplex microstructure of ordered phases [J]. Acta Materialia, 2020, 194: 106−117.

[12] NUTOR R K, XU Tian-ding, WANG Xue-lin, WANG Xiao-Dong, AN Peng-fei, ZHANG Jing, HU Tian-dou, LI Lai-feng, CAO Qing-ping, DING Shao-qing, ZHANG Dong-xian, JIANG Jian-Zhong. Liquid helium temperature deformation and local atomic structure of CoNiV medium entropy alloy [J]. Materials Today Communications, 2022, 30: 103141.

[13] ZHOU Ze-you, WU Bo, DOU Shu-shi, ZHAO Chun-feng, XIONG Yuan-peng, WU Yu-feng, YANG Shang-jin, WEI Zhen-yi. Thermodynamic properties of elements and compounds in Al−Sc binary system from ab initio calculations based on density functional theory [J]. Metallurgical and Materials Transactions A, 2014, 45: 1720−1735.

[14] HUANG Ye-yan, WU Bo, LI Fei, CHEN Li-lin, DENG Zhi-xing, CHANG Ke-ke. First-principles and CALPHAD-type study of the Ir−Mo and Ir−W systems [J]. Journal of Mining and Metallurgy, Section B: Metallurgy, 2020, 56:109118.

[15] TOGO A, TANAKA I. First principles phonon calculations in materials science [J]. Scripta Materialia, 2015, 108: 1−5.

[16] HU Kang-ming, HUANG Jin-chang, WEI Zhen-yi, PENG Qiong, XIE Zhe-yu, SA Bai-sheng, WU Bo. Elastic and thermodynamic properties of the Ti_2AlNb orthorhombic phase from first-principles calculations [J]. Physica Status Solidi (b), 2017, 254: 1600634.

[17] WANG Shen, LI Da, XIONG Jun. Prediction of elastic properties of face-centered cubic high-entropy alloys by machine learning [J]. Transactions of Nonferrous Metals Society of China, 2023, 33: 518−530.

[18] YU Wei, CHONG Xiao-yu, GAN Meng-di, WEI Yan, ZHANG Ai-min, HU Chang-yi, FENG Jing. Effect of alloying elements on thermoelastic properties of Pt-based alloys [J]. Transactions of Nonferrous Metals Society of China, 2023, 33: 157−167.

[19] WU Yi-feng, Irving D L. Finite temperature elastic properties of equiatomic CoCrFeNi from first principle [J]. Scripta Materialia, 2019, 162: 176−180.

[20] HUANG Liang-feng, LU Xue-zeng, TENNESSEN E, RONDINELLI J M. An efficient ab-initio quasiharmonic approach for the thermodynamics of solids [J]. Computational Materials Science, 2016, 120: 84−93.

[21] QIU Shi, CHEN Shu-ming, NAIHUA Nai-hua, ZHOU Jian, HU Qing-miao, SUN Zhi-mei. Structural stability and mechanical properties of B2 ordered refractory AlNbTiVZr high entropy alloys [J]. Journal of Alloys and Compounds, 2021, 886: 161289.

[22] ZHANG Hai-jun, LI Chen-hui, DJEMIA P, YANG Rui, HU Qing-miao. Prediction on temperature dependent elastic constants of “soft” metal Al by AIMD and QHA [J]. Journal of Materials Science & Technology, 2020, 45: 92−97.

[23] SANGIOVANNI D G, TASNADI F, HARRINGTON T, ODÉN M, VECCHIO K S, ABRIKOSOV I A. Temperature-dependent elastic properties of binary and multicomponent high-entropy refractory carbides [J]. Materials & Design, 2021, 204: 109634.

[24] CHEN Rong, WENG Liang-ji, ZHANG Chu-bo, ZHAO Pan-hong, SU Long-ju, XIE Tian-liang, QIAN Cheng, WU Bo, SA Bai-sheng, WEN Cui-lian, YANG Li, LIU Yu, WANG Chun-xu, YANG Xiao-lan. The influence of site preference on the elastic properties of FCC_CoCrFeNi multi-principal element alloy [J]. Journal of Alloys and Compounds, 2023, 965: 171426.

[25] ZHOU Ze-you, WU Bo, ZHENG Xiao-qing, HU Kang-ming, CHEN Kai-lu, CHEN Chao-yang, CHEN Dan, HUANG Wei-lin. First principles calculation of the ordering behavior and mechanical properties of $Al_3(Sc_{0.75}M_{0.25})$ (M=Ti, Y, Zr, Hf) intermetallic compounds [J]. Rare Metal Materials and Engineering, 2019, 48(3): 879−884. (in Chinese)

[26] ALI H, CHEN Rong, WU Bo, XIE Tian-liang, WENG Liang-ji, WEN Jian-sen, YAO Qi-peng, SU Long-ju, ZHAO Yan, ZHAO Pan-hong, SA Bai-sheng, LIU Yu, WANG Chun-xu, SU Hang, HAYAT A. The site preference and doping effect on mechanical properties of Ni_3Al-based γ' phase in superalloys by combing first-principles calculations and thermodynamic model [J]. Arabian Journal of Chemistry, 2022, 15: 104278.

[27] ALI H, CHEN Rong, CHEN Hai-lian, ZHAO Yan, ZHAO Pan-hong, YANG Shu-wen, WU Bo, WEN Jian-sen, ZHANG Chu-bo, WENG Liang-ji, XIE Tian-liang, CAI Qi, ZHANG Long-kun, HE Zhi-han, YAO Qi-peng, ZHANG Hai-feng, SA Bai-sheng, WEN Cui-lian, LIN Mao-hua, LIU Yu, WANG Chun-xu. The ordering behavior of Co_3Al-based γ' phase with $L1_2$ structure predicted by the thermodynamic model with support of first-principles calculations [J]. Materials Today Communications, 2022, 33: 104447.

[28] WU Bo, LIU Hai-long, HUANG Chao-ran, WANG Min, SU Li, ZHAO Chun-feng, ZHOU Ze-you, XIONG Yuan-peng, SHAO Yan-qun, ZHOU Bai-yang. Prediction of the site ordering behaviours of elements in C15 $NbCr_2$-based intermetallics by combining thermodynamic model with ab-initio calculation [J]. Intermetallics, 2013, 35: 104−109.

[29] WEI Zen-yi, YANG Yi-xu, HUANG Jin-chang, WU Bo, SA Bai-sheng, HUANG Ye-yan, WANG Shu-liang, LIN Mao-hua, TSAI C T, BAI Ke-wu. Prediction of site occupancy of C15 Laves phase at finite temperature based on quasi-harmonic approximation model [J]. Intermetallics, 2018, 96: 3340.

[30] WU Bo, ZINKEVICH M, ALDINGER F, SHEN Jian-yun CHU Mao-you. Prediction of the ordering behaviours of the orthorhombic phase based on Ti2AlNb alloys by combining thermodynamic model with ab initio calculation [J]. Intermetallics, 2008, 16: 42−51.

[31] WU Yu-feng, WU Bo, WEI Zhen-yi, ZHOU Ze-you, ZHAO Chun-feng, XIONG Yuan-peng, TOU Shu-shi, YANG Shang-jin, ZHOU Bai-yang, SHAO Yan-qun. Structural, half-metallic and elastic properties of the half-Heusler compounds NiMnM (M=Sb, As and Si) and IrMnAs from first-principles calculations [J]. Intermetallics, 2014, 53: 26−33.

[32] WEI Zhen-yi, TOU Shu-shi, WU Bo, BAI Ke-wu. First principle investigation of crystal lattice structure, thermodynamics and mechanical properties in $ZnZrAl_2$ intermetallic compound [J]. Solid State Communications, 2016, 247: 82−87.

[33] ZHENG Yao-dong, WU Bo, Zhang Chao-hui, DAI Pin-qiang. Prediction of the site occupations of the $ThMn_{12}$-type intermetallics $YFe_{12-x}Mo_x$ by combining thermodynamic model with ab initio calculations [J]. Intermetallics, 2010, 18, 1465−1469.

[34] ZHANG Chao-hui, LIN Mao-hua, WU Bo, YE Guo-xin, ZHANG Li-kun, CHEN Tuo, ZHANG Wen-jun, ZHENG Zhen-huan, LI Qiang, SHAO Yan-qun, ZHOU Bai-yang, WANG Chen. Explore the possibility of forming FCC high entropy alloys in equal-atomic systems CoFeMnNiM and CoFeMnNiSmM [J]. Journal of Shanghai Jiaotong University (Science), 2011, 16: 173−179.

[35] WU Bo, ZHAO Yan, ALI H, CHEN Rong, CHEN Hai-lian, WEN Jian-sen, LIU Yang, LIU Lian, YANG Kai-huan, ZHANG Long-kun, HE Zhi-han, YAO Qi-peng, ZHANG Hai-feng, SA Bai-sheng, WEN Cui-lian, QIU Yu, XIONG Hao, LIN Mao-hua, LIU Yu, WANG Chun-xu, SU Hang. A reasonable approach to describe the atom distributions and configurational entropy in high entropy alloys based on site preference [J]. Intermetallics, 2022, 144: 107489.

[36] WU Bo, XIE Zhe-yu, HUANG Jin-chang, LIN Jin-wei, YANG Yi-xu, JIANG Lin-qiao, HUANG Jiang-lin, YE Guo-xin, ZHAO Chun-feng, YANG Shang-jin, SA Bai-sheng. Microstructures and thermodynamic properties of high-entropy alloys CoCrCuFeNi [J]. Intermetallics, 2018, 93: 40−46.

[37] CHEN Rong, XIE Tian-liang, WU Bo, WENG Liang-ji, ALI H, YANG Shu-wen, ZHAO Yan, ZHAO Pan-hong, ZHANG Chu-bo, CAO Ren-hui, WEN Jian-sen, YAO Qi-peng, CAI Qi, ZHANG Hai-feng, SA Bai-sheng, WEN Cui-lian, LIN Mao-hua, SUN Xu, SU Hang, LIU Yu, WANG Chun-xu. A general approach to simulate the atom distribution, lattice distortion, and mechanical properties of multi-principal element alloys based on site preference: Using FCC_CoNiV and CoCrNi to demonstrate and compare [J]. Journal of Alloys and Compounds, 2023, 935: 168016.

[38] WENG Liang-ji, SU Long-ju, XU Neng-shen, QIAN Cheng, CAI Qi, CHEN Rong, LIU Yang, ZHAO Yan, XU Feng, ALI H, WU Bo, PENG Qiong. The preferred adsorption sites and catalytic mechanism of FCC_CoFeGaNiZn multi-principal element alloy for oxygen evolution reaction catalysis based on site preference of constituent atom on sublattice [J]. Intermetallics, 2024, 165: 108132

[39] DING Jun, YU Qin, ASTA M, RITCHIE R O. Tunable stacking fault energies by tailoring local chemical order in CrCoNi medium-entropy alloys [J]. Proceedings of the National Academy of Sciences, 2018, 115: 8919−8924.

[40] KOSTIUCHENKO T, RUBAN A V, NEUGEBAUER J, SHAPEEV A, KÖRMANN F. Short-range order in face-centered cubic VCoNi alloys [J]. Physical Review Materials, 2020, 4: 113802.

[41] CHEN Xue-fei, WANG Qi, CHENG Zhi-ying, ZHU Ming-liu, ZHOU Hao, JIANG Ping, ZHOU Ling-ling, XUE Qi-qi, YUAN Fu-ping, ZHU Jing, WU Xiao-lei, MA En. Direct observation of chemical short-range order in a medium-entropy alloy [J]. Nature, 2021, 592(7856): 712−716.

[42] CHEN Xue-fei, YUAN Fu-ping, ZHOU Hao, WU Xiao-lei. Structure motif of chemical short-range order in a medium-entropy alloy [J]. Materials Research Letters, 2022, 10: 149−155.

[43] WANG Jing, JIANG Ping, YUAN Fu-ping, WU Xiao-lei. Chemical medium-range order in a medium-entropy alloy [J]. Nature Communications, 2022, 13: 1021.

[44] CAI Wei-jin, HE Jun-yang, WANG Li, YANG Wen-chao, XU Xiang-qi, YAQOOB K, WANG Zhang-wei, SONG Min. Characterization of chemical short-range order in VCoNi medium-entropy alloy processed by spark plasma sintering [J]. Scripta Materialia, 2023, 231: 115463.

[45] MONIRI S, YANG Yao, DING Jun, YUAN Ya-kun, ZHOU Ji-han, YANG Long, ZHU Fan, LIAO Yu-xuan, YAO Yong-gang, HU Liang-bing, ERCIUS P, MIAO Jian-wei. Three-dimensional atomic structure and local chemical order of medium- and high entropy nanoalloys [J]. Nature, 2023, 624: 564−569.

[46] ZUNGER A, WEI S H, FERREIRA L G, BERNARD J E. Special quasirandom structure [J]. Physical Review Letters, 1990, 65: 353−356.

[47] VAN DE WALLE A. Multicomponent multisublattice alloys, nonconfigurational entropy and other additions to the alloy theoretic automated toolkit [J]. Calphad, 2009, 33: 266−278.

[48] KRESSE G, FURTHMUELLER J. Efficiency of ab-initio total energy calculations for metals and semiconductors using a plane-wave basis set [J]. Computer Materials Science, 1996, 6: 15−50.

[49] PERDWE J P, BURKE K, ERNZERHOF M. Generalized gradient approximation made simple [J]. Physical Review Letter, 1996, 77: 3865−3868.

[50] KRESSE G, FURTHMUELLER J. Efficient iterative schemes for ab-initio total-energy calculations using a plane-wave basis set [J]. Physical Review B, 1996, 54: 11169−11186.

[51] KRESSE G, JOUBERT J. From ultra-soft pseudo-potentials to the projector augmented-wave method [J]. Physical Review B, 1999, 59: 1758−1775.

[52] MONKHORST H J, PACK J D. Special points for Brillouin-zone integrations [J]. Physical Review B, 1976, 13: 5188−5192.

[53] ZHOU Xiao, TEHRANCHI A, CURTIN W A. Mechanism and prediction of hydrogen embrittlement in fcc stainless steels and high entropy alloys [J]. Physical Review Letters, 2021, 127: 175501.

[54] MOUHAT F, COUDERT F X. Necessary and sufficient elastic stability conditions in various crystal systems [J]. Physical Review B, 2014, 90: 224104.

[55] SENKOV O N, MIRACLE D B. Generalization of intrinsic

ductile-to-brittle criteria by Pugh and Pettifor for materials with a cubic crystal structure [J]. Scientific Reports, 2021, 11: 4531.

[56] TIAN Yong-jun, XU Bo, ZHAO Zhi-sheng. Microscopic theory of hardness and design of novel superhard crystals [J]. International Journal of Refractory Metals and Hard Materials, 2012, 33: 93−106.

[57] WEI Zhen-Yi, HU Kang-Ming, SA Bai-Sheng, WU Bo. Pressure-induced structure, electronic, thermodynamic and mechanical properties of Ti_2AlNb orthorhombic phase by first-principles calculations [J]. Rare Metals, 2021, 40: 1−11.

[58] SARKER P, HARRINGTON T, TOHER C, OSES C, SAMIEE M, MARIA J P, BRENNER D W, VECCHIO K S, CURTAROLO S. High-entropy high-hardness metal carbides discovered by entropy descriptors [J]. Nature communications, 2018, 9: 4980.

[59] LI Qi-kang, HUANG Zhuo-bin, XIE Ming-da, YE Wen-ting, ZHOU Qing, QIU Long-shi, QIAN Dan, PINTO H C, SONG Zhong-xiao, WANG Hai-feng. A VCoNiN multi-principal nitride film with excellent wear performance [J]. Surface and Coatings Technology, 2023, 475: 130130.

有序化行为对 FCC_CoNiV 多主元合金热力学和力学性能的影响

张楚波[1]，钱 程[2]，叶子安[2]，赵攀红[1]，陈 荣[2]，吴 波[1,2]，乔 阳[1]，
翁良基[1]，苏龙菊[2]，谢天良[2]，萨百晟[2]，刘 雨[3]，王春旭[3]

1. 福州大学 先进制造学院 材料设计与制造模拟实验室，晋江 362200；
2. 福州大学 材料科学与工程学院 多尺度材料设计实验室 材料基因工程研究所，福州 350100；
3. 钢铁研究总院 高温合金研究院，北京 100081

摘 要：采用对比研究方法，以 FCC_CoNiV 多主元合金(MPEAs)为案例，研究了多主元合金的有序态构型和无序态构型的随温度变化的热力学性质和力学性质。有序态构型的搭建是基于先前预测的该多主元合金的原子占位分数(SOFs)；而无序态构型的搭建则基于传统特殊准随机结构(SQS)假设。结果表明，有序化行为不仅提高了合金相结构的热力学稳定性，而且提高了弹性性能和维氏硬度。例如，对于基于 SOFs 的有序化构型，在 973 K 下，预测获得的体积弹性模量(B)、剪切模量(G)，杨氏模量(E)以及维氏硬度(H_V)分别为 187.82 GPa、79.03 GPa、207.93 GPa 和 7.58 GPa；而对于基于 SQS 的无序化结构，相应力学性能数据分别为 172.58 GPa、57.45 GPa、155.14 GPa 和 4.64 GPa。基于有序化结构预测获得的硬度值与实验值吻合良好，而基于无序态结构预测得到的硬度值被明显低估。

关键词：FCC_CoNiV；多主元合金(MPEAs)；有序化行为；随温度变化的性能；计算材料科学

(Edited by Bing YANG)